KeA1

CHINESE ROOTS
GLOBAL IMPACT

Contents lists available at ScienceDirect

# **Bioactive Materials**

journal homepage: www.keaipublishing.com/en/journals/bioactive-materials





# Robust adhesion between solid-state hydroxyapatite and bone tissue through surface demineralization

Shichao Xie <sup>a</sup>, Masahiro Okada <sup>b,\*</sup>, Haruyuki Aoyagi <sup>a</sup>, Akihisa Otaka <sup>a</sup>, Xiaofeng Yang <sup>a</sup>, Takayoshi Nakano <sup>c</sup>, Takuya Matsumoto <sup>a,\*\*</sup>

- <sup>a</sup> Department of Biomaterials, Graduate School of Medicine, Dentistry and Pharmaceutical Sciences, Okayama University, 2-5-1 Shikata-cho, Kita-ku, Okayama City, Okayama. 700-8558. Japan
- Division of Biomaterials Science and Engineering, Graduate School of Dentistry, Tohoku University, 4-1 Seiryo-machi, Aoba-ku, Sendai City, Miyagi, 980-8575, Japan
- c Division of Materials and Manufacturing Science, Graduate School of Engineering, The University of Osaka, 2-1 Yamadaoka, Suita City, Osaka, 565-0871, Japan

#### ARTICLE INFO

#### Keywords: Solid-state adhesive Hydroxyapatite Demineralized bone Collagen Hydration

#### ABSTRACT

*Objective:* Current bone adhesives typically lack adequate mechanical strength, long-term stability, or biocompatibility. To address these limitations, we designed a new adhesion strategy using a solid-state hydroxyapatite (HAp) adhesive in combination with bone surface demineralization.

Methods: Solid-state HAp adhesives were synthesized via wet chemical precipitation and heat treatment. Cortical bone specimens were partially demineralized with phosphoric acid (H<sub>3</sub>PO<sub>4</sub>) or ethylenediaminetetraacetic acid (EDTA), and characterized using scanning electron microscopy (SEM) and attenuated total reflectance–Fourier transform infrared spectroscopy (ATR-FTIR). Shear adhesion strength of HAp to demineralized bone was measured over time. In vivo fixation was assessed in rats using micro-computed tomography and histology. Statistical analysis used Tukey-Kramer tests after normality and variance checks.

Results: Although the HAp adhesive failed to adhere to non-demineralized bone, effective adhesion was achieved on the surface-demineralized bone tissue. Shear adhesion strength was significantly higher in EDTA-treated samples (238.4 kPa at 10 h) compared to  $\rm H_3PO_4$ -treated samples (102.9 kPa at 1 h), with performance correlating with demineralization depth. ATR-FTIR and SEM analyses revealed that EDTA preserved collagen's triplehelix structure and free water content, both enhancing adhesion. Animal experiments confirmed stable fixation of HAp adhesive to demineralized bone tissue.

Conclusions: Surface demineralization enabled strong adhesion of the solid-state HAp adhesive to bone by exposing collagen swollen with water. Adhesion strength was influenced by structural changes in the demineralized layer, and the adhesive provided stable *in vivo* fixation, supporting its potential for bone-anchored biomedical applications.

## 1. Introduction

Devices that need to be fixed to the bone surface—such as orthopedic plates used for fracture fixation [1] and sensors employed to assess *in vivo* skeletal mechanical properties [2,3]—require stable attachment to the bone surface. Current strategies for device fixation primarily rely on invasive physical methods (e.g., bone screws) [1–4] or adhesive materials [5–7]. Commonly used bone adhesives, including methyl

methacrylate (MMA) bone cement [8,9], fibrin glues [10,11], and polyurethane-based bone cements [12,13], have demonstrated favorable bone tissue adhesion. However, these adhesives often suffer from limitations such as lack of biodegradability (in the case of MMA), poor long-term adhesion stability [14], and insufficient mechanical strength [15], thus failing to meet the stringent requirements for efficient fixation on hard tissues. As a result, developing bone tissue adhesives remains a significant challenge, requiring the simultaneous optimization of

Peer review under the responsibility of editorial board of Bioactive Materials.

E-mail addresses: masahiro.okada.c2@tohoku.ac.jp (M. Okada), tmatsu@md.okayama-u.ac.jp (T. Matsumoto).

<sup>\*</sup> Corresponding author. Division of Biomaterials Science and Engineering, Graduate School of Dentistry, Tohoku University, Miyagi, Japan.

<sup>\*\*</sup> Corresponding author. Department of Biomaterials, Graduate School of Medicine, Dentistry and Pharmaceutical Sciences, Okayama University, Okayama, Japan.

sustained adhesion strength, mechanical robustness, and biocompatibility.

Bioactive ceramic materials—such as hydroxyapatite (HAp), tricalcium phosphate (TCP), calcium phosphate bone cements, and bioactive glass-have long attracted widespread attention for orthopedic applications [16-18]. HAp, the primary inorganic component of bone tissue, has attracted particular attention. Recently, Okada et al. developed a novel solid-state adhesive: a porous HAp-based material capable of adhering to soft connective tissues, such as dermis rich in type I collagen (Col-1), under wet conditions [19]. Compared with glue-type materials, the solid-state HAp adhesive offers advantages such as ready-to-use properties without the need for curing. The HAp adhesive exhibited superior adhesion strength compared to commercial fibrin glue [19]. Additionally, they demonstrated that the adhesion strength could be modulated by adjusting the pore structure of the HAp adhesives [20]. However, while the HAp adhesive displayed effective adhesion to biological soft tissues, it did not exhibit adhesion to hard tissues such as bone, significantly restricting its utility as a bone adhesive.

Bone tissue is composed of  $\sim 30$  % organic material (predominantly Col-1),  $\sim 60$  % inorganic material (predominantly HAp), and  $\sim 10$  % water [21–23]. When the inorganic component is completely removed via demineralization, Col-1 becomes exposed and water occupies the resultant voids. We hypothesized that the surface of demineralized bone would resemble soft connective tissue and therefore could facilitate adhesion of the porous HAp adhesive. Of note, although both dermal tissues and demineralized bones are predominantly composed of Col-1, structural differences such as Col-1 fiber orientation and cross-linking density [24] would have an impact on adhesion efficacy.

Demineralization is widely employed in clinical dental treatments and for the preparation of decalcified histological sections of hard tissues. In dental treatments, phosphoric acid  $(H_3PO_4)$  [25] and ethylenediaminetetraacetic acid (EDTA) [26,27] are often used to remove smear layers consisting of mineral debris from enamel surfaces and root canals, respectively. Hydrochloric acid (HCl) and formic acid (HCOOH) are commonly used in histological decalcification of bone [26].

In this study, we investigated the effects of surface demineralization on bone tissue and its influence on the adhesion behavior of the HAp adhesive. As demineralizing agents, HCl and HCOOH were excluded in this study because of their volatility and harmfulness [28,29]. Instead,  $\rm H_3PO_4$  and EDTA were employed as demineralizing agents, given their established use in clinical dentistry and proven safety and efficacy profiles. Furthermore, we evaluated the *in vivo* fixation of the HAp adhesive to demineralized bone tissue and examined the potential for long-term attachment.

# 2. Materials and methods

## 2.1. Materials

Unless otherwise specified, all materials used in this study were of reagent grade and purchased from FUJIFILM Wako Pure Chemical Corporation (Osaka, Japan). Ultrapure Milli-Q water (Millipore Corp, Bedford, MA, USA) was used in all experiments.

## 2.2. Preparation of HAp adhesives

Following a previously reported method [20], HAp nanoparticle water dispersion was prepared via wet chemical synthesis method at room temperature ( $\sim\!25\,^{\circ}\text{C}$ ). After washing and degassing the dispersion (9 wt%) under reduced pressure for 30 s, approximately 240  $\mu\text{L}$  was poured into a white-petrolatum-coated silicone mold (10 mm diameter  $[\varphi]\times 2$  mm thickness) and dried at 80 °C for 3 h. The resulting HAp adhesive (approximately 5 mm $\varphi\times 1$  mm thickness) was soaked in anhydrous ethanol for 12 h and washed three times with anhydrous ethanol to remove residual petrolatum. After washing and drying, the HAp adhesive was heated at 600 °C for 1 h (heating rate: 10 °C/min).

The diameter of the HAp adhesives was controlled by changing the diameter of silicone mold. The HAp adhesive with different thickness (0.25, 0.5 or 1.5 mm) was prepared by grinding one surface of the HAp adhesive (1.0 mm thickness or 2.0 mm thickness prepared by using the double amount of dispersion) with #3000 silicon carbide abrasive papers (Buehler, Illinois Tool Works Inc., IL, USA) under Milli-Q water irrigation. After grinding, the HAp adhesive was washed with Milli-Q water and dried at 80  $^{\circ}$ C for 12 h. In the following adhesion test, the unground surface of HAp adhesive was attached on each tissue.

## 2.3. Surface demineralization of bone tissues

Cortical femoral bone from slaughtered barrows (~6 months old; weight: 100-120 kg; Tokyo Shibaura Zoki KK., Tokyo, Japan) was cut with a diamond saw and ground to 15 mm  $\times$  10 mm  $\times$  2 mm using #3000 silicon carbide abrasive paper under water irrigation. Each bone specimen weighed ~0.60 g. To ensure consistency in the initial condition of each specimen, Vickers hardness (HV) was measured with a tester (FM-700; Future Tech Corp., Tokyo, Japan) at 25 g-force (gf) for 15 s. Specimens with hardness in the range of 35-45 HV [30] were used in this study. Bone specimens were placed in 12-well culture plates, and 3 mL of EDTA (5, 10, or 17 %; pH = 7.45) or  $H_3PO_4$  (1, 5, or 10 %) was added per well. Demineralization was performed at 37 °C for 0.5, 1, 2, or 3 h (and 5 or 10 h in the case of EDTA). After treatment, specimens were rinsed three times in excess ultrapure water (20 s each) and stored in Milli-Q water at 4 °C for up to 48 h. For rapid demineralization screening, H<sub>3</sub>PO<sub>4</sub> at higher concentration (10, 30, 50, or 70 %) was also tested for 10 min.

To measure demineralization depth, bone specimens were ground from its side until the non-demineralized area was exposed, and observed using a reflected light polarizing microscope (MM 11U; Nikon Corp., Tokyo, Japan). An image analysis software (ImageJ; NIH, MD, USA) was used to measure the demineralization depth (sample size (N) = 3). To validate the accuracy of this measurement method with more objective method, the micro-computed tomography (CT, Latheta LCT200; HITACHI Corp., Tokyo, Japan) observation of the same sample was performed, and the demineralization depth was calculated from the CT image by using a thickness analysis option in a CT data analysis software (VGStudio Max 2.2, Volume Graphics GmbH, Heidelberg, Germany) with the thresholds of demineralized areas set between -400 and 1800 from the CT measurement of fully demineralized bones.

Surface and cross-sectional morphologies of the demineralized bone tissue were observed using scanning electron microscope (SEM, S-4800; HITACHI Corp., Tokyo, Japan). After demineralization, specimens were fixed with 4 % paraformaldehyde for 12 h and with 2 % osmium tetroxide solution for 3 h, dehydrated with 70 % and 100 % ethanol and tert-butyl alcohol, and then freeze-dried. The samples used for cross-sectional observation were broken perpendicular to their long axis after freeze-drying. Each sample was coated with osmium (Neoc-Pro; Meiwafosis Co., Ltd., Tokyo, Japan). Collagen fibril diameter was measured form cross-sectional images using ImageJ (N = 27).

Infrared spectra of the bone tissue surface before and after demineralization (without fixation, dehydration, freeze-drying or osmium coating) were obtained using an attenuated total reflectance–Fourier transform infrared spectroscopy (ATR-FTIR, IRAffinity-1S; Shimadzu Corp., Kyoto, Japan) at 40 % relative humidity (RH) at room temperature ( $\sim$ 25 °C). Spectra were analyzed using a peak fitting software (OriginPro2024; OriginLab, Northampton, MA, USA).

## 2.4. Adhesion test with porcine femur section or mouse dermis in vitro

A preliminary experiment was performed using a porcine femur section (thickness: 8.8 mm; weight: 4.9 g) after its outer surface was planarized with #3000 silicon carbide abrasive paper, and demineralized using 300  $\mu L$  of 10 %  $H_3PO_4$  at 37  $^{\circ}C$  under 100 % RH for 3 h. After thoroughly rinsing the bone surface with distilled water, excess moisture

was removed using filter paper, and a HAp adhesive was applied to the demineralized area, pressed at 15 N for 15 s, and then lifted using tweezers.

Next, adhesion strength was quantitatively measured using bone specimens demineralized under the conditions described in the previous section 2.3. After removing residual water and using the same adhesive application protocol, the bone was clamped to the upper side of a mechanical tester (EZ test; Shimadzu Corp., Kyoto, Japan), and a stainless-steel baffle was positioned just above the HAp adhesive without contact to the bone specimen. The contact between the stainless-steel baffle and the HAp adhesive was assumed to be a line contact due to its circularity of the HAp adhesive. The maximum loading rate of 150 mm/min of the mechanical tester was chosen in this study to minimize the effects of elastic relaxation at the demineralized layer-HAp interface [31]. The apparent shear adhesion strength was calculated based on the maximum load (detachment force) divided by the adhesion area (N = 3).

In order to observe the interfacial adhesion state between HAp and demineralized bone specimen, the sample without fixation nor further demineralization was immediately embedded into a cryo-embedding compound (Tissue-Tek O.C.T. compound; Sakura Finetek, California, USA). The cross sections with 8  $\mu m$  in thickness were prepared using the Kawamoto method [32] with a cryostat (CM3050S; Leica Biosystems Nussloch GmbH, Nussloch, Germany) at a microtome internal temperature of  $-35~^{\circ}\text{C}$  and a sample stage temperature of  $-45~^{\circ}\text{C}$ . Sections were stained with hematoxylin and eosin (H&E) and observed under an optical microscope. The condensation layer thickness was measured from the images (N = 3).

The influence of demineralization on mechanical strength of bone was evaluated by using a single-surface demineralized bone specimens with  $10\,\%\,H_3PO_4$  under the same conditions described in subsection 2.3, after all other surfaces were protected from the contact with demineralizing solutions by applying tapes (NW-15SF, Nichiban Co. Ltd., Tokyo, Japan). After removing the tapes, the protected (i.e., non-demineralized) surface was confirmed and the demineralized depth on the demineralized surface was measured from the optical microscope observations. A three-point bending test was then performed with the demineralized surface facing upward at a support span of 10 mm under a loading rate of 1 mm/min at room temperature (N = 5).

To achieve a shorter demineralization, higher concentrated  $\rm H_3PO_4$  (10, 30, 50, or 70 %) was used and the treatment time was set to 10 min, which is required to complete polymerization of PMMA bone cement [33]. The demineralization depth measurement, ATR FT-IR measurement and SEM observation were performed as described in subsections 2.3. The shear adhesion strength with the HAp adhesive was also measured by the same methods described above.

Adhesion tests using mice dermis were also performed under the same conditions as described in a previously reported method [20]. In the case of HAp adhesives with different thicknesses prepared by grinding one surface of the adhesive, the unground surface of adhesive was attached on each tissue (N = 3). The interfacial adhesion state between HAp and dermis was observed, and the thickness of condensation layer formed on dermis was measured from the frozen sections (N = 3) prepared according to the method described above.

## 2.5. Adhesion test with rat femur in vivo

All animal experiments involving rats and mice were conducted in strict accordance with the guidelines for animal experimentation at the corresponding author's institution, following approval by the institutional review board (protocol no. OKU-2023046). In this study we selected 12-week(w)-old female SD rats because bone remodeling in rats has essentially reached a steady state, as demonstrated in the literature [34]. By using a well-characterized and uniform skeletal stage model, we minimized biological differences between species, thereby improving our understanding of HAp fixation on demineralized bone.

The HAp adhesives were sterilized in an autoclave (High Clave HVE-

50, Hirayama Manufacturing Corp., Saitama, Japan) at 120 °C for 20 min after sealing in a sterile roll bag (HM-1305, Hogy Medical Co. Ltd., Tokyo, Japan). The sterilized HAp adhesive was then stored in a vacuum bag at room temperature. To verify the influence of autoclave sterilization on the adhesion properties of HAp adhesive, in vitro dhesion test was conducted with the autoclaved HAp adhesives stored at room temperature for 1 month (m) and the demineralized bone tissues with 50 %  $\rm H_3PO_4$  at 10 min (N = 3). The control group received no treatment (N = 3).

After anesthetizing a 12-w-old female Sprague-Dawley rat (Shimizu Laboratory Supplies Co., Ltd., Kyoto, Japan), an incision was made in the left hind limb. After removal of the periosteum, a hole ( $\phi$  3.0 mm  $\times$ 1.0 mm depth) was drilled on the lateral aspect of the femoral knee joint. In order to prevent spreading the demineralizing agent to unintended areas, we used a sponge (approximately 2.5 mm  $\times$  2.5 mm  $\times$  2 mm) prepared from a hydrophilic polytetrafluoroethylene membrane filter (0.2 µm in thickness, H020A047A; ADVANTEC Toyo Kaisha, Ltd., Japan) folded six times and cut into the block-shaped sponge. After soaking the sponge in 50 % H<sub>3</sub>PO<sub>4</sub> and removing the excess fluid, the sponge was placed in the hole to demineralize for 10 min. After the hole was then rinsed with saline, and excess moisture was absorbed using sterile surgical gauze (RS4-30; Osaki Medical, Nagova, Japan), the HAp adhesive ( $\phi$  2.8 mm  $\times$  1.0 mm depth) was inserted into the hole under a pressure (~15 N) followed by applying a small volume of blood obtained from the surrounding tissue, and then the incised skin was sutured using absorbable sutures with sterile needle (Nesco suture; Alfresa Pharma Corp., Osaka, Japan) (N = 6). As a control group, demineralization was not applied after the hole was drilled (N = 6). Of note, the diameter of HAp adhesive ( $\phi$  2.8 mm) was set to be smaller than that of hole ( $\phi$  3.0 mm) in order to facilitate the displacement of HAp adhesive and to prevent interference caused by size-related mechanical interlocking. The autologous blood was applied on the exposed HAp surface after the implantation to prevent the adhesion to epithelial or muscular tissues during implantation experiments. In order to confirm the anti-adhesion effect of blood coating, a small volume of blood (~4 μL) obtained from the mouse carotid artery was applied to the single-surface of the HAp adhesive and then the shear adhesion test was performed with mice dermis (N = 3) under the same conditions as described in subsection 2.3 and non-coated HAp adhesives were used as a control (N = 3).

The micro-CT (Latheta LCT200) measurements of the knee joints at 0 days (d), 1 d, 1 week (w), and 1 month (m) after surgery were performed (N = 6). The displacement of HAp adhesives at 1 w was quantitatively evaluated from the angular deviation of the HAp adhesives at the position of the HAp adhesive on 0 d as the baseline (i.e.,  $0^{\circ}$  at 0 d). After the bone tissue containing the HAp adhesive was harvested and the surrounding muscle tissue was cleaned off, H&E-stained cryosections were prepared as described in subsection 2.3. The inflammatory response and the osteoconductivity of HAp adhesive were evaluated from the histological observation, and the contact area (%) between new bone and HAp at 1 m was calculated as an osteoconductivity index by ImageJ software (N = 6).

To evaluate the influence of demineralization on the mechanical strength of rat femurs (12-w-old female Sprague-Dawley rat), the harvested femur was immersed in 50 % phosphoric acid (15 mL) at 37 °C for 10 min, and then three-point bending test was performed (N = 5) at a support span of 10 mm and a loading rate of 1 mm/min at room temperature. The bending strength ( $\sigma$ ) was calculated from the following equation (1) under the simple assumption femur was a cylinder [35]:

$$\sigma = 32FL / \{4\pi (D_0^4 - D_i^4)/D_0\}$$
 (1)

where F is the maximum load, L is the support span,  $D_o$  is the outer diameter and  $D_i$  is the inner diameter, respectively.

#### 2.6. Statistical analysis

Data are expressed as mean  $\pm$  standard deviation (SD). Normality and homogeneity of variances were calculated using the Shapiro–Wilk and Bartlett tests, respectively. Group comparisons were conducted using the Tukey–Kramer test. All statistical analyses were performed using R software (version 4.4.2; R Core Team, 2024) with a significance level set at  $\alpha=0.05$ .

## 3. Results and discussion

## 3.1. HAp adhesives

In this study, HAp adhesives subjected to heat treatment at 600  $^{\circ}$ C were used, as they exhibited an optimal porosity for soft tissue adhesion while demonstrating double the mechanical strength of non-treated HAp [20]. While HAp adhesives with a square plate shape were evaluated in the previous studies [19,20], a circular disk shape (Fig. S1A) was used in this study to avoid stress concentration at the interface of adhesive and tissue [36,37]. Notably, comparative analysis of soft tissue (i.e., mice dermis) adhesion strength between the two external shapes revealed no significant difference (Fig. S1B), indicating that the adhesive performance of HAp plates exhibits minimal correlation with their external shape.

Regarding the adhesion mechanism of the HAp adhesive on soft tissues (such as dermis), the following factors were proposed [19,20]: (i) Ionic and molecular interactions:  $\text{Ca}^{2+}$  and  $\text{PO}_4^{3-}$  ions on the surface of HAp crystals form ionic and molecular interactions with collagen fibers in the soft tissue matrix. (ii) Capillary action: the inherent microporous channels in the HAp adhesive induce capillary action (i.e., autonomous

absorption of interstitial fluid from the soft tissue). (iii) Collagen condensation: Fluid migration leads to the accumulation and densification of collagen fibers, forming a condensed collagenous layer that amplifies ionic and molecular interactions. Of note, the contribution of capillary action of porous HAp adhesive used in this study was estimated to be 74 % (and 26 % was contributed by ionic and molecular interactions) from the reduced adhesion strength (14.7 kPa) of the dense (non-porous) HAp adhesive compared with that (56.3 kPa) of porous HAp adhesive onto mice dermis [20]. The porosity of HAp adhesive was directly proportional to both the condensed collagenous layer thickness (that was related to the water absorption amount) and the adhesion strength at the same volume of HAp adhesives [20]. Although the thickness of HAp adhesive is expected to have an impact on the adhesion strength because the thickness is related to the total pore volume (and hence to the water absorption amount), the adhesion strength was not changed at the same porosity when the thickness was above 0.25 mm (Fig. S2). This would be because the condensation layer formed on mice dermis was constant (around 40 um regardless of the thickness of HAp as shown in Fig. S2C) hence 0.25 mm (250 µm) thickness of the HAp adhesive was enough to absorb water from the tissue surface. Of note, the HAp adhesive with less than 0.25 mm thickness could not be prepared due to brittleness of porous HAp used in this study. In the following experiments, the HAp adhesives with 1 mm thickness were used.

## 3.2. HAp adhesion to demineralized bone tissue

HAp adhesives could not adhere to non-demineralized bone surfaces, and thus their adhesion strength could not be measured. To preliminarily assess the effect of demineralization, a part of porcine femur surface was treated with  $10\ \%\ H_3PO_4$  for  $3\ h$ . It was confirmed that HAp

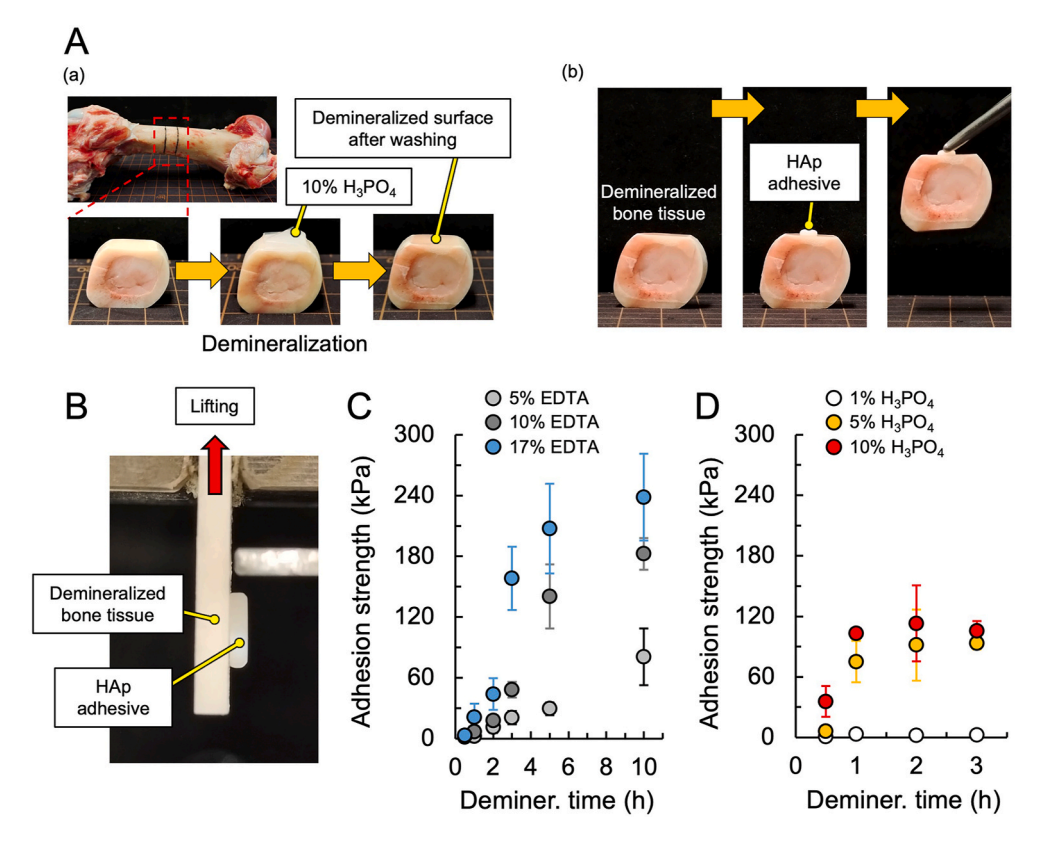


Fig. 1. HAp adhesion on demineralized bone. A) Digital images during the preliminary experiment of HAp adhesion on demineralized bone tissue: (a) The middle part of a porcine femur was cut, and a 10~% H $_3$ PO $_4$  solution was applied on the surface for 3~h; (b) After surface demineralization, a HAp adhesive was placed on the bone surface, and the adhesive was lifted while adhering to the bone. B) Digital image of the shear adhesion test setup. C–D) Apparent shear adhesion strengths of HAp adhesives on bone tissues after demineralization with C) EDTA and D) H $_3$ PO $_4$  solutions at different time points (N = 3). Error bars indicate standard deviations. Abbreviations: HAp, hydroxyapatite; H $_3$ PO $_4$ , phosphoric acid; EDTA, ethylenediaminetetraacetic acid.

adhesives could adhere to surface-demineralized bone within 15 s (Fig. 1A and Supplementary Video V1). This immediate adhesion is not mediated by biologically active cellular processes but rather by physical interactions and/or chemical bonding at the demineralized bone–HAp interface.

Next, the effects of demineralization solution (type and concentration) and treatment time were evaluated quantitatively using shear adhesion tests (Fig. 1B). The results demonstrated that the adhesion

strength of HAp plates increased with longer demineralization times and reached to a maximum depending on the demineralization solution used (Fig. 1C and D). For example, with 17 % EDTA, maximum adhesive strength reached 238.4 kPa, although a prolonged demineralization time (10 h) was required (Fig. 1C). In the case of lower concentration EDTA, it took longer to reach the adhesion strength similar to that of 17 % EDTA (e.g., 158.3 kPa for 17 % EDTA at 3h, 140.3 kPa for 10 % at 5 h). In contrast, 1 % H<sub>3</sub>PO<sub>4</sub> resulted in low adhesion strength (3.2 kPa),

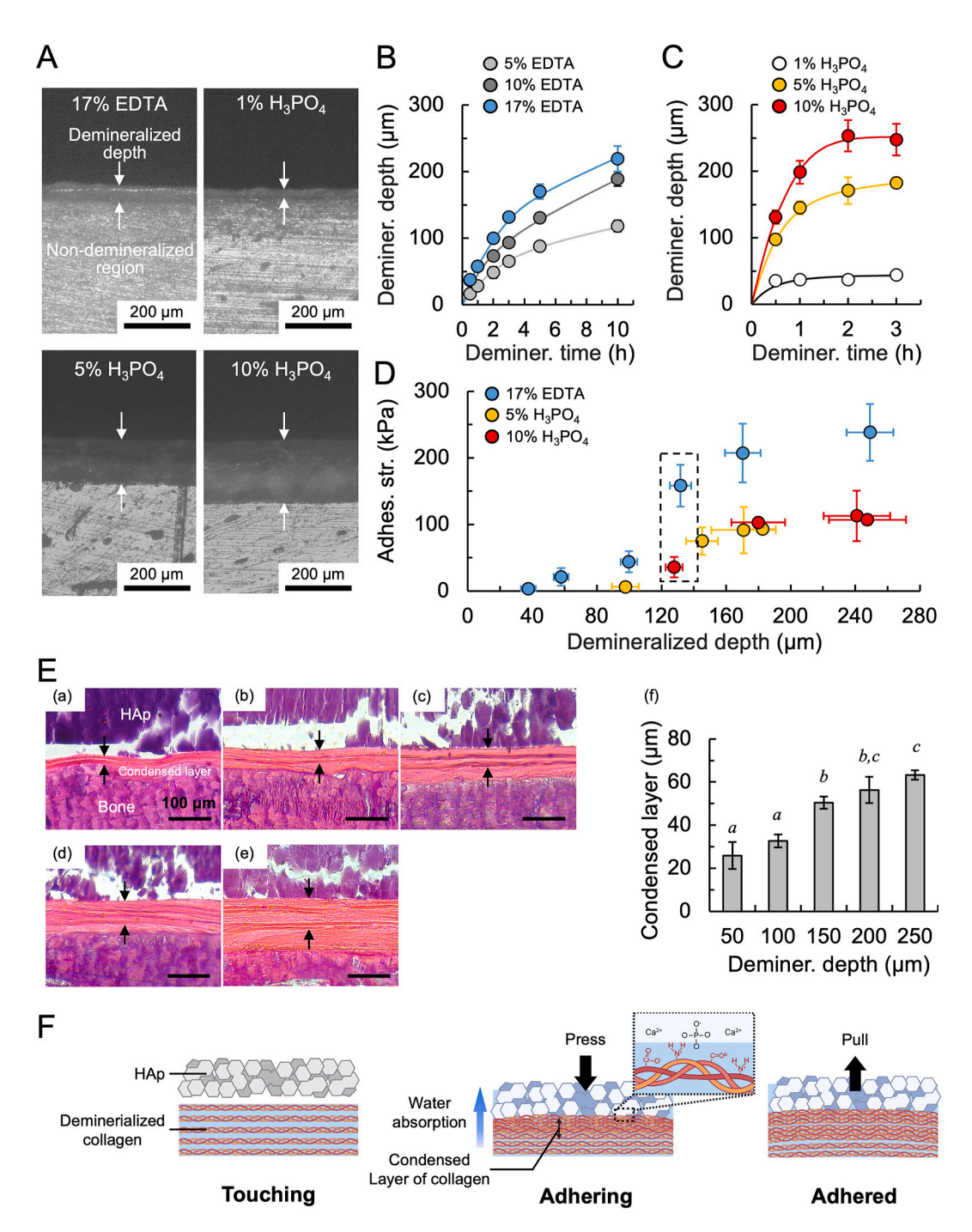


Fig. 2. Demineralization depth and adhesion strength. A) Optical micrographs of bone cross sections after demineralization for 1 h with different solutions. Arrows indicate demineralization depths. Time evolution of demineralization depth with B) EDTA and C)  $H_3PO_4$  and solutions (N = 3). D) Relationship between the demineralization depth and adhesion strength of HAp. E) H&E-stained cross sections of demineralized bones attached with HAp, showing the condensation layers (arrows) on the demineralized bone having different demineralized depths ( $\mu$ m): (a) 50, (b) 100, (c) 150, (d) 200, and (e) 250, and (f) relationship between the demineralization depth and the thickness of condensed layer (N = 3). Different italic letters (a, b and c) on the bars indicate statistically significant differences. Error bars indicate standard deviations. F) Schematic diagram illustrating the adhesion mechanism between demineralized bone tissue and HAp. Abbreviations: EDTA, ethylenediaminetetraacetic acid;  $H_3PO_4$ , phosphoric acid; HAp, hydroxyapatite.

likely caused by insufficient demineralization. When using 5 % and 10 %  $\rm H_3PO_4$ , maximum adhesive strengths of 91.5 kPa and 102.9 kPa were achieved after 1 h and 0.5 h of treatment, respectively, suggesting that the total  $\rm H^+$  ion concentration influences demineralization efficiency (Fig. 1D). These results highlight the need to understand how different demineralization solutions affect the adhesion strength between HAp and bone tissue.

Of note, the adhesion strength of HAp adhesive onto demineralized bone specimen (maximum, 238.4 kPa with EDTA) was significantly larger than that onto dermis (~60 kPa in this study; Fig. S1B and S2B). The dermis, prioritized for elasticity and extensibility, possesses a relatively loose collagen architecture and its extracellular matrix comprises also elastic fibers and reticulin fibers (type III collagen) [24], which facilitate stretching but confer lower ultimate tensile strength [38]. In contrast, bone's load-bearing function necessitates a tightly packed collagen arrangement, resulting in high toughness and limited extensibility [39], which means that demineralized bone lacks elastic fiber-like collagens and is instead composed of non-collagenous components, including proteoglycans and structural glycoproteins [40]. The tightly packed architecture and superior mechanical strength of demineralized bone would contribute significantly to its adhesion strength with HAp adhesives. However, the adhesion strength of a single piece of current HAp adhesive was at several hundred kPa, which would be insufficient to orthopedic plate fixation application. Therefore, current HAp adhesive should be used in non-load-bearing applications (e.g., fixation of small biosensors and binder of bone fragments etc.).

#### 3.3. Characterization of demineralized bone surface

The demineralization surface was observed from the cross-sectional view (Fig. 2A). In optical micrographs, the reflective white region corresponded to non-demineralized bone, while a translucent dark region-attributed to residual organic matrix-was observed after demineralization. These features were consistent with those reported by Veronika et al. [41]. The translucent dark region formed after the treatment with 10 % H<sub>3</sub>PO<sub>4</sub> for 1 h was observed with SEM (Fig. S3), and complete HAp disappearance in the top or middle areas was confirmed. However, incomplete removal was observed at the boundary between the non-demineralized and demineralized areas (Fig. S3). This boundary region likely represents a propagating "reaction front," a transition zone characterized by a gradient in Ca and P concentrations [41]. Notably, when sufficient demineralization solution amount is available, the demineralization rate decreases and stabilizes with the front progression due to (a) depletion of demineralizing solution near the reaction front, and (b) diminished calcium/phosphate (Ca<sup>2+</sup>/PO<sub>4</sub><sup>3-</sup>) ion diffusion efficiency [42,43]. In this study, the volume of demineralizing solution was relatively small (demineralizing solution: 3 mL; bone specimen: 0.60 g), which likely led to a progressive reduction in demineralization rate, ultimately limiting the depth of demineralization.

The demineralization depth was measured from the cross-sectional observations (Fig. 2A). Of note, the demineralization depth measured from the cross-sectional observation was almost the same as those measured from CT image ( $R^2 = 0.9901$ ; Fig. S4A and B). At the same demineralization duration, significant differences in demineralization depth were observed among samples treated with different solutions (Fig. 2A). In this study, under conditions of insufficient solution volume (demineralizing solution: 3 mL; bone specimen: 0.60 g), comparative analysis of time-dependent demineralization depth profiles (Fig. 2B and C) revealed that the depth in the H<sub>3</sub>PO<sub>4</sub>-treated group increased rapidly and subsequently stabilized within a short period. In contrast, the EDTAtreated group exhibited a slower rate of demineralization, consistent with our prediction. Assuming the following: (1) the apparent density of cortical bone is  $2 \text{ g/cm}^3$  [44,45]; (2) the inorganic content of bone is 65 wt% [22]; (3) the inorganic component is stoichiometric HAp; (4) demineralization initiates from the bone surface [41,42]; (5) phosphate ions dissolve as dihydrogen phosphate (H<sub>2</sub>PO<sub>4</sub>) at pH 0.70 (in the case

of 10 %  $H_3PO_4$ ), with a  $H_2PO_4$ /hydrogen phosphate (HPO<sub>4</sub><sup>2-</sup>) ratio of  $3.03 \times 10^6$  [46]; and (6) CaEDTA<sup>2-</sup> complexes form in the case of EDTA treatment, theoretical demineralization depths were calculated to be 42  $\mu m$  for 1 %  $H_3PO_4$ , 211  $\mu m$  for 5 %  $H_3PO_4$ , 442  $\mu m$  for 10 %  $H_3PO_4$ , 99  $\mu m$  for 5 % EDTA 198  $\mu m$  for 10 % EDTA and 336  $\mu m$  for 17 % EDTA. The experimentally measured demineralization depths were 38 µm for 1 % H<sub>3</sub>PO<sub>4</sub>, 176  $\mu$ m for 5 % H<sub>3</sub>PO<sub>4</sub>, 250  $\mu$ m for 10 % H<sub>3</sub>PO<sub>4</sub>, 118  $\mu$ m for 5 % EDTA189  $\mu m$  for 10 % EDTA and 249  $\mu m$  for 17 % EDTA. At 1 % H<sub>3</sub>PO<sub>4</sub> concentration, the experimental result closely matched theoretical predictions. Conversely, at elevated H<sub>3</sub>PO<sub>4</sub> concentrations (5 % and 10 %), acidic disintegration and degradation of collagen fibers [47] likely occurred, consuming acid and thereby limiting further mineral dissolution—resulting in smaller demineralization depths than the calculated values. For EDTA, the demineralization depth did not stabilize even after 10 h of treatment, due to its gradual chelation kinetics [25].

Based on the adhesion mechanism of the HAp adhesive on soft tissues (such as dermis) described in 3.1, the contents of collagen fibers and water at the bone surface after demineralization (i.e., the demineralization depth) affect the adhesion strength of the HAp adhesive on demineralized bone. Therefore, the correlation between demineralization depth and adhesion strength was plotted (Fig. 2D), excluding 1 % H<sub>3</sub>PO<sub>4</sub> (due to its minimal demineralization depth) and 5 %/10 % EDTA (due to the similarity to 17 % EDTA). Adhesion strength started to increase at a depth of ~100 μm across all groups. Beyond 160 μm, it plateaued, with distinct differences observed between the H<sub>3</sub>PO<sub>4</sub> and EDTA groups. In order to clarify this phenomenon, the adhesive interfaces between the HAp adhesives and bone tissues with varying demineralization depths were observed (Fig. 2E), and condensed layers were also confirmed on the demineralized bone surfaces. Of note, due to the limited extensibility of demineralized bone compared with dermis as discussed in 3.2, the condensed layer of demineralized bone was observed as a compressive light-dark striations under the microscopic observation. The quantitative analysis shown in Fig. 2E(f) demonstrated that for demineralization depths below 100 µm, the condensed layer thickness remained relatively small at approximately 30 µm due to the limited water migration from thin demineralized area. The condensed layer thickness increased to approximately  $50-60 \mu m$  by increasing the demineralization depths from 100 to 150 µm, and remained constant above the demineralization depth of 150 µm, which might indicate the saturation of water migration. This variation in the condensed layer thickness correlated with the adhesion strength shown in Fig. 2D. Based on the aforementioned findings, the adhesion mechanism between the HAp adhesive and demineralized bone tissue was summarized (Fig. 2F). Consistent with previous conclusions [20], when the HAp adhesive contacted the demineralized bone surface, it spontaneously absorbed fluids, including water, from the demineralized tissue via capillary action. Concurrently, collagen fibers at the interface adsorbed to the HAp surface through ionic and molecular interactions.

Of note, the demineralization could also affect the mechanical properties of bone itself. Therefore, three-point bending tests were performed with the 10 %  $H_3PO_4$ . treated bone specimens having demineralization depths. The results (Fig. S4C) indicated that there is no significant difference in bending strength below the demineralization depth of 150  $\mu m$ , and the strength decreased from 84.5 MPa to 58.3 MPa at the demineralized depth of 250  $\mu m$ . By integrating these data with the adhesion strength shown in Fig. 2D, the optimal demineralization depth would be approximately 150  $\mu m$ .

By comparing specimens at similar demineralization depths, the 10 %  $\rm H_3PO_4$  and 5 %  $\rm H_3PO_4$  groups demonstrated statistically similar adhesive strengths, whereas the EDTA-treated group consistently exhibited greater adhesion strength than the  $\rm H_3PO_4$ -treated groups. At a demineralization depth of ~130  $\rm \mu m$ , a statistically significant difference in adhesion strength was first observed between the 10 %  $\rm H_3PO_4$  and EDTA groups (p=0.05). These findings suggest that, in addition to demineralization depth as a primary factor, the structural state of the

demineralized tissue also influenced adhesion of HAp adhesives, because acid treatment induces structural alterations in the organic matrix (e.g., denaturation and dissolution), leading to swelling and subsequent influx of additional water into the tissue [47–49]. Therefore, surface organic matrices of demineralized bone specimens (with 130  $\mu m$  depth) treated with 17 % EDTA for 3 h and 10 %  $H_3PO_4$  for 0.5 h were analyzed.

SEM was employed to analyze morphological alterations on bone

tissue surfaces. Non-demineralized samples (i.e., samples after grinding the top surface with #3000 silicon carbide abrasive papers) exhibited a large number of spherical HAp crystals encapsulating collagen fibrils in both top surface and cross-sectional views in Fig. 3A(a–c), making the collagen fibril outlines difficult to discern. This morphology likely reflects the bone mineralization process, during which HAp crystals also form within intrafibrillar regions [50]. Collagen fibrils were clearly visible on the top surface of EDTA-treated specimens as shown in Fig. 3A

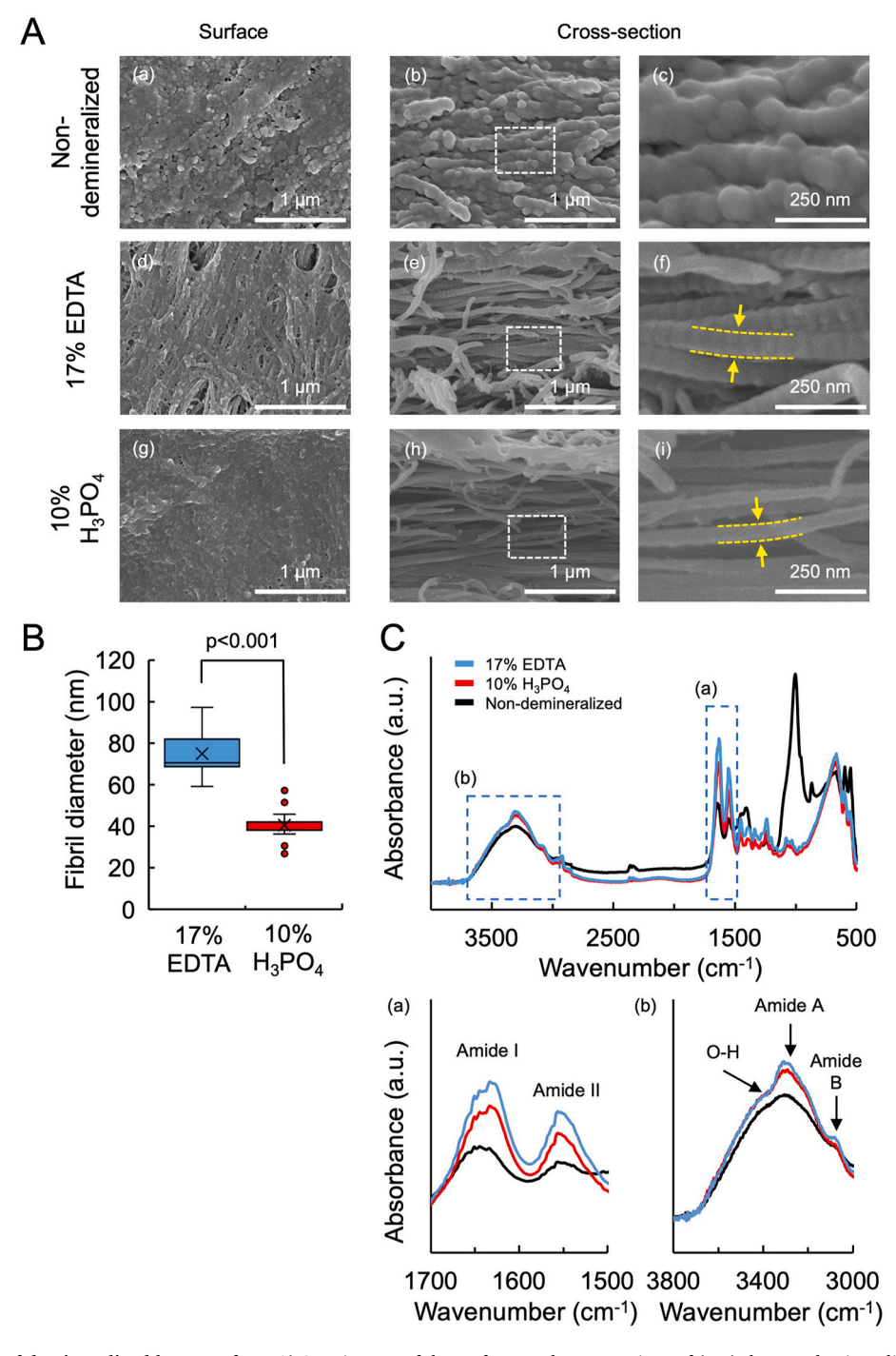


Fig. 3. Characterization of demineralized bone surface. A) SEM images of the surfaces and cross-sections of (a–c) the non-demineralized and the demineralized bone tissues with (d–f)  $10 \% H_3PO_4$  for 0.5 h and (g–i) 17 % EDTA for 3 h at the same demineralization depth ( $130 \mu m$ ). The dashed boxes in (b, e, f) indicate the magnified location shown in (c, f, i), respectively. The arrows indicate the diameter of collagen fibrils. B) Diameter of collagen fibrils (N = 27). Error bars indicate standard deviations. C) Representative ATR-FTIR spectra of the untreated and demineralized bone tissues surfaces with  $10 \% H_3PO_4$  for 0.5 h and 17 % EDTA for 3 h spectra at (a) amide I/II band and (b) OH + NH stretching band regions. Abbreviations: SEM, scanning electron microscopy; HAp, hydroxyapatite;  $H_3PO_4$ , phosphoric acid; EDTA, ethylenediaminetetracetic acid; ATR-FTIR, attenuated total reflectance–Fourier transform infrared spectroscopy.

(d), whereas fibrils were not observed on the top surface of H<sub>3</sub>PO<sub>4</sub>-treated group as shown in Fig. 3A(g), supporting collagen degradation by H<sub>3</sub>PO<sub>4</sub> [49]. Although fibrils were evident in the cross-sectional views of both groups as shown in Fig. 3A(e,f) and 3A(h,j), the collagen fibril diameter in the H<sub>3</sub>PO<sub>4</sub> group was significantly smaller than in the EDTA-treated samples (Fig. 3B). These findings confirm acid-induced structural degradation of collagen during H<sub>3</sub>PO<sub>4</sub> demineralization, and explain the discrepancy between experimentally measured and theoretically calculated demineralization depths in the H<sub>3</sub>PO<sub>4</sub>-treated group. Acidic environments induce collagen fiber alternations sequentially through swelling, structural disintegration, and ultimate degradation, accompanied by characteristic changes in fibril diameter (i.e., initial thickening followed by thinning prior to complete degradation) [47,51]. In contrast, EDTA-mediated demineralization proceeds via chelation of Ca<sup>2+</sup> ions from HAp crystals, causing minimal disruption to collagen structure and thereby effectively preserving its architectural integrity [46].

ATR-FT-IR spectroscopy was employed to quantitatively analyze the differences in collagen secondary structures among the demineralized bone groups, using non-demineralized bone tissue as a reference to assess structural alterations. The decreased intensity of the  $PO_4^{3-}$  peak near  $1000~cm^{-1}$  after demineralization further supports the disappearance of HAp in the dementalized layers, in agreement with SEM observations, and the ATR-FTIR spectra exhibited enlarged collagen-associated amide I/II bands in the  $1500-1700~cm^{-1}$  range, indicating collagen exposure (Fig. 3C). The intensities of. amide I/II bands in the  $H_3PO_4$  group were lower than those in the EDTA group (Fig. 3C(a)), whereas the intensities of O–H stretching vibrations of water were similar (Fig. 3C(b)), suggesting a higher degree of water-induced swelling in the  $H_3PO_4$  group compared to the EDTA group.

Deconvolution of infrared spectra within the amide I band was performed to assess collagen secondary structures, following established methodologies [52]. Characteristic absorption peaks were assigned as follows:  $\alpha$ -helix ( $\sim$ 1656 cm<sup>-1</sup>),  $\beta$ -turn ( $\sim$ 1616 and 1667 cm<sup>-1</sup>),  $\beta$ -sheet

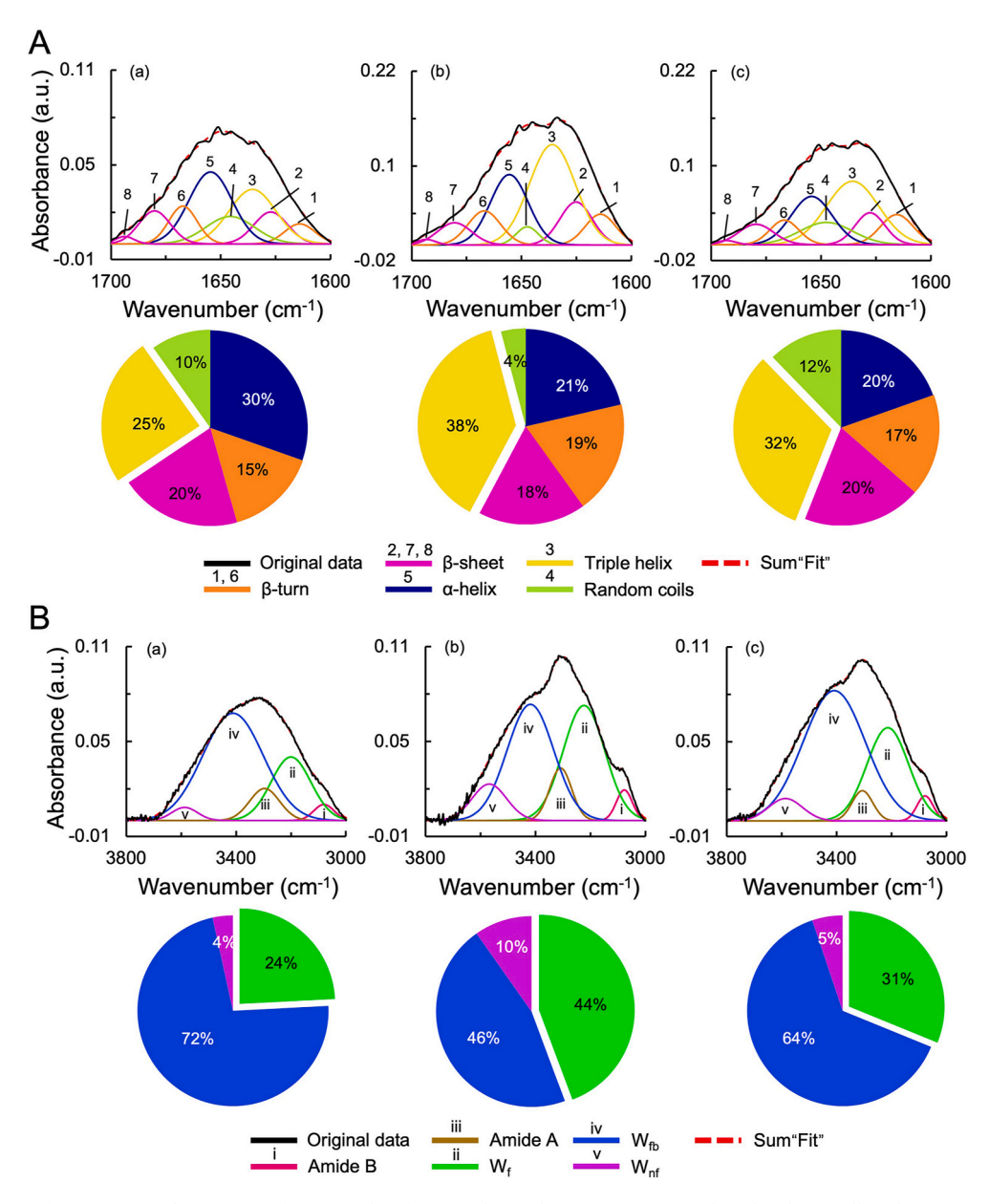


Fig. 4. Deconvolution of IR spectra of bone. Curve fitting results of (A) amide I and (B) OH + NH stretching bands as well as the proportion of each secondary structure of collagen fibril and each hydrating water structures for (a) non-demineralized and (b,c) demineralized bone tissues with (b) 17 % EDTA for 3 h and (c) 10 %  $H_3PO_4$  for 0.5 h at the same demineralization depth (130  $\mu$ m). Abbreviations: EDTA, ethylenediaminetetraacetic acid;  $H_3PO_4$ , phosphoric acid;  $W_{fb}$  freezing water;  $W_{fb}$ , freezing bound water;  $W_{nf}$ , non-freezing bound water.

 $(\sim 1626, 1680 \text{ and } 1694 \text{ cm}^{-1})$ , triple helix  $(\sim 1636 \text{ cm}^{-1})$ , and random coils (~1645 cm<sup>-1</sup>) (Fig. 4A). In this study, the structural integrity of collagen was evaluated based on the proportions of triple helix and random coil (Fig. 4A-Table S1). Prior to demineralization, the mineral phase in bone tissue produces a contraction stress in collagen fibrils, causing the structure change of the fibrils and dehydration [53,54]. Therefore, the non-demineralized bone exhibited a triple helix content of 25 %, while the demineralized groups exhibited increased triple helix contents (EDTA group, 38 %; H<sub>3</sub>PO<sub>4</sub> group, 32 %). Comparative analysis revealed the lowest proportion of random coils in the EDTA-treated group (4 %), whereas the H<sub>3</sub>PO<sub>4</sub> group (12 %) exhibited higher levels than the non-demineralized controls (10 %). Regarding the proportion of α-helix, both demineralized groups showed reduced levels relative to controls (non-demineralized group, 30 %; EDTA group, 21 %; and H<sub>3</sub>PO<sub>4</sub> group, 20 %). Notably, β-sheet/turn configurations demonstrated minimal alterations across the groups. The observed structural transformation of collagen after demineralization may be attributed to fibril relaxation induced by HAp dissolution, accompanied by the recovery of D-spacing and hydration structure. This restoration process facilitates reestablishment of hydrogen bonds, thereby restoring the secondary structure of the collagen fibrils to the non-mineralized state [54–57]. However, in the case of H<sub>3</sub>PO<sub>4</sub> treatment, collagen decomposition is also evident [47-49,55]. Statistical analysis indicated significant differences in triple helix, random coil, and α-helix content among groups (Fig. S5A). In correlation with the adhesion strength results shown in Fig. 2D, the triple helix and α-helix contents exhibited positive correlations with adhesion strength, whereas random coil content showed a negative correlation.

These structural alterations in collagen fibrils inevitably influence the structure of hydrating water. In this study, hydrating water was classified into freezing water (Wf), freezing bound water (Wfb), and nonfreezing bound water (Wnf) [58], depending on their degree of interaction with organic molecules. Deconvolution of the O-H and N-H stretching bands (3000-3800 cm<sup>-1</sup>) was performed according to established methodologies [40,48]. Characteristic absorption peaks were assigned as follows:  $W_f$  (~3210 cm<sup>-1</sup>),  $W_{fb}$  (~3400 cm<sup>-1</sup>), and  $W_{nf}$  $(\sim 3590 \text{ cm}^{-1})$  [58], in addition to amide A  $(\sim 3300 \text{ cm}^{-1})$  and amide B  $(\sim 3075 \text{ cm}^{-1})$  bands [59] (Fig. 4B). The results were summarized in Table S2. Wnf, which interacts strongly with organic molecules and exhibits the lowest mobility, was more abundant in the EDTA group (Wnf, 10 %) than in the H<sub>3</sub>PO<sub>4</sub> group (W<sub>nf</sub>, 5 %). Generally, structurally intact collagen fibrils bind tightly to water through their helical structure and internal polar groups (such as N-H, C=O), enabling W<sub>nf</sub> to occupy the spaces between triple helices [60,61], resulting in a relatively higher W<sub>nf</sub> content in the EDTA group. Wfb, which weakly interacts with organic molecules and has low mobility, was more prominent (Wfb, 64 %) in the H<sub>3</sub>PO<sub>4</sub> group than in the EDTA group (W<sub>fb</sub>, 46 %). Disruption of the helical structure by H<sub>3</sub>PO<sub>4</sub> exposes internal polar groups [60], potentially increasing the content of W<sub>fb</sub>. W<sub>f</sub>, which has mobility similar to bulk water and does not interact with organic molecules, was higher (W<sub>f</sub>, 44 %) in the EDTA group than in the H<sub>3</sub>PO<sub>4</sub> group (W<sub>f</sub>, 31 %), indicating that  $W_{\rm f}$  was transformed to  $W_{\rm fb}$  due to helical structure disruption, in the H<sub>3</sub>PO<sub>4</sub> group. Notably, the total water content—estimated from the combined  $W_f + W_{fb} + W_{nf}$  peak areas—was slightly lower in the EDTA group (33.3) than in the H<sub>3</sub>PO<sub>4</sub> group (36.4). However, the W<sub>f</sub> content was greater in the EDTA group (33.3  $\times$  0.44 = 14.7) than in the  $H_3PO_4$  group (36.4 × 0.31 = 11.3) (Table S2). Statistical analysis indicated significant differences in each hydrating water component (Fig. S5B). The W<sub>f</sub> and W<sub>nf</sub> ratios positively correlated with adhesion strength, whereas W<sub>fb</sub> exhibited a negative correlation.

Next, we discuss the impact of the above-described alterations in collagen secondary structure on adhesion strength. Different demineralization solutions, due to their different demineralization mechanisms, determine the conformation of collagen fibrils, and the distribution of surface chemical groups. Specifically, the use of strong acids (such as phosphoric acid) with low pH values (<1) can cause collapse and

irreversible hydrolysis of the collagen fibrils. Overhydration can also affect the fibril arrangement, further compromising structural stability. While these changes can provide sufficient adhesion sites for the HAp adhesive in a short period of time, the adhesion strength is reduced due to the destruction of the collagen fibril structure. EDTA forms a coordination bond with Ca<sup>2+</sup> in HAp in bone tissue and gradually disintegrates the crystal structure of HAp, and can better preserve the structure of the fibrils (triple helix structure, etc.) and mechanical integrity. Although the demineralization rate of EDTA is much lower than that of acidic agents, this makes the surface of bone tissue relatively stable after demineralization, which is conducive to achieving long-term and effective adhesion. The influence of demineralization mechanism discussed here is consistent with the influence of etching mechanism on adhesion strength of dental adhesives [25]. Water migration from the tissue into the porous HAp adhesive is also one of the key factors [19. 20]. Therefore, a high content of W<sub>f</sub> with higher mobility is favorable for adhesion. In contrast, Wfb has been reported to prevent adsorption on solid surfaces [58]; hence, lower W<sub>fb</sub> content is preferable. These hydrating water structures are related to collagen structural integrity (i.e., high triple helix content and low random coil content). Moreover, collagen structural integrity contributes to mechanical strength, which is another important factor in maintaining strong adhesion. Notably, the slight increase in total water content observed in H<sub>3</sub>PO<sub>4</sub> group may adversely affect mechanical strength, because an increase in water content progressively reduces the mechanical properties of collagen [62], and collagen disrupted or swollen by H<sub>3</sub>PO<sub>4</sub> demonstrates poor tensile strength [60-62]. Consequently, the adhesion strength between the H<sub>3</sub>PO<sub>4</sub>-treated samples and the HAp adhesive was significantly lower than that observed in the EDTA-treated group.

## 3.4. Adhesion test with rat femur in vivo

Integrating the above findings, comparative analysis revealed that the H<sub>3</sub>PO<sub>4</sub>-treated groups required significantly shorter demineralization durations than the EDTA-treated groups. The primary objective of this study was to establish fundamental in vivo fixation protocols for living bone surfaces. Considering both operational practicality and the requirement for rapid adhesion, H<sub>3</sub>PO<sub>4</sub> was selected as the demineralizing agent, and we further investigated the effect of its concentration, using a fixed duration of 10 min, which is required to complete polymerization of PMMA cement [33]. In the context of clinical validation, high-concentrated (65 %) H<sub>3</sub>PO<sub>4</sub> has been used for dental applications [63]. Based on this clinical precedent and our experimental design, the maximum concentration employed in this study was set at 70 %, with additional gradients of 50 % and 30 %. Of note, the application of high-concentrated (10-70 %) H<sub>3</sub>PO<sub>4</sub> entails potential risks, because excessive PO<sub>4</sub><sup>3-</sup> exposure may disrupt phosphate homeostasis, potentially inducing hyperphosphatemia, phosphate toxicity, and tissue damage such as hypocalcemia [64,65]. These risks necessitate careful operational protocols during demineralization, including the prevention of acid spreading to unintended areas and the thorough irrigation with physiological saline to eliminate residual acidity.

After 10 min of demineralization, comparative analysis of demineralization depths revealed that 70 %  $\rm H_3PO_4$  produced the shallowest layer, while no significant differences were observed among the other concentrations (Fig. 5A). This was likely due to high viscosity of 70 %  $\rm H_3PO_4$  (13.9 mPa s), which impedes deep tissue penetration, compared to 50 %  $\rm H_3PO_4$  (5.1 mPa s) at 25 °C [66]. Regarding adhesion, both the 50 % and 70 %  $\rm H_3PO_4$  groups demonstrated adhesive capability, with the 50 %  $\rm H_3PO_4$  group achieving 25 kPa (Fig. 5B). Of note, the present adhesion strength of HAp adhesive under the above conditions was larger than that of fibrin glue (12.1 kPa [67]) but was lower than that of PMMA bone cements (25 MPa [8]).

ATR-FTIR analysis showed that the 70 %  $H_3PO_4$  group exhibited significantly higher intensities in the 3000–3800 cm<sup>-1</sup> range (indicative of increased water content, Fig. 5C(b)) and lower amide I band

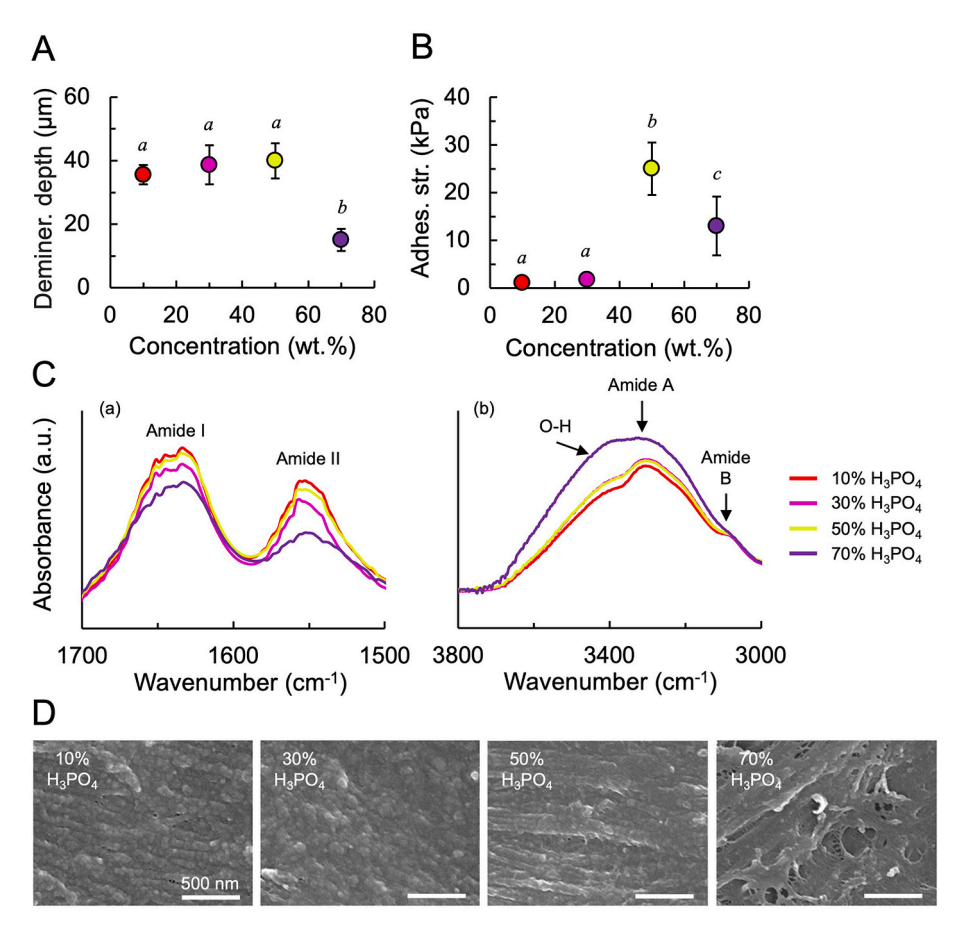


Fig. 5. Demineralization with concentrated  $H_3PO_4$  for 10 min. A) Demineralized depths and B) apparent shear adhesion strengths of HAp on demineralized bone with different concentration of  $H_3PO_4$  (N = 3). Error bars indicate standard deviations and different italic letters (a, b and c) on the bars indicate statistically significant differences. C) ATR-FTIR spectra at (a) amide I/II band and (b) OH + NH stretching band regions, and D) SEM images of the demineralized bone with different concentration of  $H_3PO_4$ . Abbreviations: HAp, hydroxyapatite;  $H_3PO_4$ , phosphoric acid; ATR-FTIR, attenuated total reflectance–Fourier transform infrared spectroscopy SEM, scanning electron microscopy.

intensities (Fig. 5C(a)) compared to other conditions, suggesting severe organic matrix degradation and swelling. These results from the 70 %  $\rm H_3PO_4$  group align with our findings in the previous subsection: disruption of collagen fibril structure leads to reduced adhesion strength. Additionally, SEM observations confirmed severe structural compromise in the organic matrix in the 70 %  $\rm H_3PO_4$  group (Fig. 5D). Collectively, these results reinforce the conclusion that demineralization depth is a fundamental factor governing adhesion to HAp adhesive, while changes in collagen fibril structure and water phase composition also significantly affect the adhesion strength.

Based on the above results, we conducted a feasibility study by fixing the HAp adhesive in a bone defect after demineralization with 50 % H<sub>3</sub>PO<sub>4</sub> for 10 min (Fig. 6A). We set the observation period from 0 d to 1 m because we focused on the initial adhesion (within several seconds) and longer-term osteoconductive fixation of HAp because the osteoconduction of rat models is completed within 3-4 w [68]. Of note, the HAp adhesive was implanted after the autoclave sterilization and storage (within 1 m). Therefore, the adhesive strength of the HAp adhesive was checked after the autoclave sterilization and storage for 1 m, and we confirmed that the sterilized samples showed the same adhesion strength as non-sterilized controls (Fig. S6A). Besides, to prevent non-specific adhesion to epithelial or muscle tissues after the implantation, the HAp surface, which was not attached to the bone surface, was coated with a small quantity of autologous blood. This treatment effectively prevented unwanted adhesion to soft tissues (Fig. S6B). We also assessed the impact of the 10-min demineralization with 50 % H<sub>3</sub>PO<sub>4</sub> on the mechanical strength of bone tissues from three-point

bending tests with entire rat femurs, and there was no significant difference in the strength before and after the demineralization (Fig. S6C).

To accurately investigate the fixation state of the HAp adhesive and the osteoconductivity of HAp adhesive, we utilized micro-CT scans and histological cross-sectional analysis (Fig. 6B and C). Micro-CT images revealed that the HAp adhesive slightly migrated within 24 h after implantation in the control group without demineralization, whereas it remained fixed in the demineralized bone tissue (Fig. 6B: 0 and 1 d). Histological sections demonstrated that the HAp adhesive adhered directly to the bone tissue, forming a condensed collagenous layer (Fig. 6C: 0 and 1 d). This phenomenon aligns with the previous in vitro findings, indicating that the adhesion mechanism of the HAp adhesive to demineralized bone in vivo is essentially the same as that observed on in vitro. Micro-CT images acquired at 1 w and post-implantation showed that the control group exhibited significant displacement, which became more pronounced at 1 m (Fig. 6B: 1 w and 1 m). In contrast, the adhesive fixed to demineralized bone maintained its position (Fig. 6B: 1 w and 1 m). The angular displacement of the HAp adhesive was quantified from the CT images at 1 w, and it was shown that the demineralized group showed no significant deviation, whereas the control group exhibited an angular displacement of approximately 12.8° (Fig. 6D). Histological sections at 1 w post-implantation (Fig. 6C: 1 w) revealed that the HAp adhesive in both groups was encapsulated by fibrous connective tissue, a natural feature of the bone defect healing process, which included abundant osteoblasts and fibroblasts [69,70]. Images acquired after 1 m showed that the connective tissue at the interface between the HAp adhesive and the demineralized bone had disappeared and was replaced

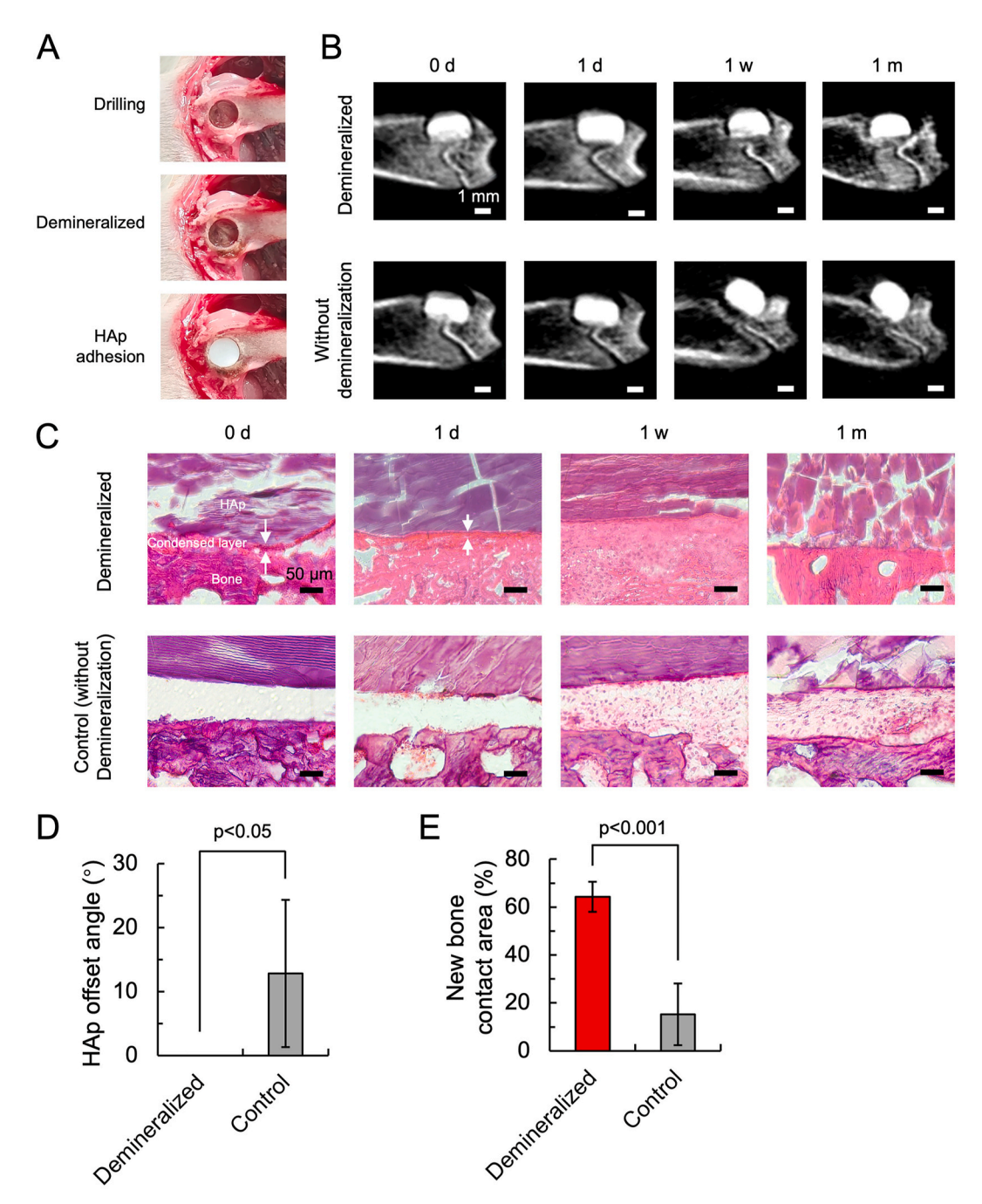


**Fig. 6. Fixation of HAp adhesive on bone** *in vivo.* A) Digital images during the animal experimental process. B) Micro-CT images and C) H&E-stained cross sections of bone tissues with HAp adhesives at different implantation periods. D) Angular deflection of the HAp adhesive after implantation for 1 w (N = 6). E) Bone-contact ratio between the HAp adhesive and newly formed bone after implantation for 1 m (N = 6). The control test was performed without demineralization. Abbreviations: Micro-CT, micro-computed tomography; H&E, Hematoxylin and Eosin; HAp, hydroxyapatite; d, day(s); w, week(s); m, month(s).

by newly formed bone tissue (Fig. 6C: 1 m). In contrast, the control group showed no significant remodeling compared to the 1-w time point, with interfacial gaps between HAp and bone tissues. The presence of interfacial gaps likely facilitated soft tissue infiltration, leading to the formation of fibrocartilage-like connective tissue [70], and this tissue subjected the HAp adhesive to continuous mechanical disturbance during bone remodeling, ultimately resulting in displacement. To evaluate the osteoconductivity of the HAp adhesive, we quantitatively evaluated the bone-implant (HAp, in this study)-contact area from the H&E-stained sections at 1 m according to the literature [71], and it was shown that the bone-implant contact area (64.4 %) was significantly higher than that (15.2 %) in the control group (Fig. 6E). Based on the

above results, the HAp fixed on the demineralized bone is expected to prevent the initial displacement due to immediate adhesion in a short term and to stabilize the fixation in a long-term due to the osteoconductivity of HAp. The osteoconductivity is the inherent property of HAp, whereas traditional MMA bone cement is bioinert and its exothermic nature during polymerization [8] may cause thermal necrosis of surrounding bone tissue. Fibrin glue also does not promote new bone formation and must be combined with other bioactive components to facilitate bone integration [72].

Although this study demonstrates encouraging results, several limitations should be acknowledged. In vivo experiments were conducted exclusively on a limited number of small, single-species models. This

may yield outcomes divergent from those in medium-to-large species (e. g., humans), potentially affecting adhesive behavior and consequently limiting extrapolation to broader clinical applications and biological contexts. Furthermore, the observation period primarily focused on early post-implantation stages. The long-term implications for bone remodeling/integration remain unelucidated, as does a comprehensive understanding of biological performance (e.g., quantitative degradation kinetics, biomechanical property assessments) and potential immune responses. For the application of HAp adhesives to fixation of device on bone tissues, some modifications should be required. For instance, glue type adhesives should be applied to combine the device and HAp adhesives, and the shape of HAp adhesive should be changed to fit the target device's geometry. These issues warrant careful investigation in future studies.

#### 4. Conclusions

This study successfully achieved stable adhesion between bone tissue and the HAp adhesive using a demineralization-based approach. Treatment with different demineralizing solutions induced distinct alterations in bone structure, which in turn differentially impacted adhesion strength. Among the organic matrix components, preservation of the triple-helix structure showed a positive correlation with the adhesion strength of HAp on demineralized bone. In addition, the presence of freezing water played a dominant role in facilitating rapid adhesion. Furthermore, we demonstrated that the HAp adhesive enables long-term positional stability through its adhesion to demineralized bone, suggesting its utility as a robust fixation material for bone sensors and other hard tissue applications, providing new strategies and broader application prospects for bone repair and other biological monitoring.

## CRediT authorship contribution statement

**Shichao Xie:** Writing – original draft, Visualization, Investigation, Data curation. **Masahiro Okada:** Writing – review & editing, Validation, Project administration, Methodology, Funding acquisition,

Conceptualization. Haruyuki Aoyagi: Methodology, Investigation. Akihisa Otaka: Validation, Methodology. Xiaofeng Yang: Investigation. Takayoshi Nakano: Validation, Supervision, Conceptualization. Takuya Matsumoto: Writing – review & editing, Validation, Supervision, Project administration, Methodology, Funding acquisition, Conceptualization.

#### Data statement

The data that support the findings of this study are available from the corresponding author upon reasonable request.

## Ethics approval and consent to participate

All animal experiments involving rats and mice were conducted in strict accordance with the guidelines for animal experimentation at Okayama University, following approval by the institutional review board (protocol No. OKU-2023046).

#### **Declaration of competing interest**

Takayoshi Nakano is an associate editor for Bioactive Materials and was not involved in the editorial review or the decision to publish this article. All authors declare that there are no competing interests.

## Acknowledgements

This work was supported by KAKENHI (grant numbers: JP23H00235, JP23K24532, JP24K02626, JP24K22187 and JP25K22163) from Japan Society for the Promotion of Science and by CREST (grant number: JPMJCR22L5) from Japan Science and Technology Agency.

The graphical abstract and Fig. 2D were respectively created with BioRender.com (license numbers: XE2909CKCV and FN290FGCJ1).

We would like to thank Editage (www.editage.jp) for English language editing.

## Glossary

НАр	hydroxyapatite
MMA	methyl methacrylate
EDTA	ethylenediaminetetraacetic acid
TCP	tricalcium phosphate
Col-1	type I collagen
HCl	hydrochloric acid
$H_3PO_4$	phosphoric acid
НСООН	formic acid
SEM	scanning electron microscopy
ATR-FTIR	attenuated total reflectance-Fourier transform infrared spectroscopy
Micro-CT	micro-computed tomography
d, w, m	day(s), week(s), month(s)
HV	Vickers hardness
RH	relative humidity
H&E	hematoxylin and eosin
$W_f$	freezing water
$W_{\mathrm{fb}}$	freezing bound water
$W_{nf}$	non-freezing bound water

# Appendix A. Supplementary data

Supplementary data to this article can be found online at https://doi.org/10.1016/j.bioactmat.2025.11.030.

#### References

- [1] G. Chandra, A. Pandey, S. Pandey, Design of a biodegradable plate for femoral shaft fracture fixation, Med. Eng. Phys. 81 (2020) 86–96, https://doi.org/10.1016/j. medengphy.2020.05.010.
- [2] A.M. Rich, W. Rubin, S. Rickli, T. Akhmetshina, et al., Development of an implantable sensor system for in vivo strain, temperature, and pH monitoring: comparative evaluation of titanium and resorbable magnesium plates, Bioact. Mater. 43 (2025) 603–618, https://doi.org/10.1016/j.bioactmat.2024.09.015.
- [3] A. Najafzadeh, L. Wong, D.S. Gunawardena, et al., Biomechanical assessment and quantification of femur healing process using fibre bragg grating strain sensors, Sens. Actuators A Phys. 347 (2022) 113930, https://doi.org/10.1016/j. sna.2022.113930.
- [4] R. Agarwal, V. Gupta, J. Singh, Additive manufacturing-based design approaches and challenges for orthopaedic bone screws: a state-of-the-art review, J. Braz. Soc. Mech. Sci. Eng. 44 (1) (2022) 37, https://doi.org/10.1007/s40430-021-03331-8.
- [5] H.B. Bingol, J.C.M.E. Bender, J.A. Opsteen, et al., Bone adhesive materials: from bench to bedside, Mater. Today Bio 19 (2023) 100599, https://doi.org/10.1016/j. mtbio.2023.100599.
- [6] A. Kirillova, C. Kelly, N. von Windheim, K. Gall, Bioinspired mineral-organic Bioresorbable bone adhesive, 7, https://doi.org/10.1002/adhm.201800467, 2018.
- [7] H. Guo, W. Zhang, Z. Jia, et al., A biodegradable supramolecular adhesive with robust instant wet adhesion for urgent hemostasis and wound repair, Adv. Funct. Mater. 34 (29) (2024) 2401529, https://doi.org/10.1002/adfm.202401529.
- [8] V.S. Seesala, L. Sheikh, B. Basu, S. Mukherjee, Mechanical and bioactive properties of PMMA bone cement: a review, ACS Biomater. Sci. Eng. 10 (10) (2024) 5939–5959, https://doi.org/10.1021/acsbiomaterials.4c00779.
- [9] S. Ramanathan, Y.C. Lin, S. Thirumurugan, et al., Poly (methyl methacrylate) in orthopedics: strategies, challenges, and prospects in bone tissue engineering, Polymers 16 (3) (2024) 367, https://doi.org/10.3390/polym16030367.
- [10] T.S. Santos, R.P.F. Abuna, A.L.G. Almeida, et al., Effect of collagen sponge and fibrin glue on bone repair, J. Appl. Oral Sci. 23 (6) (2015) 623–628, https://doi. org/10.1590/1678-775720150374.
- [11] V.V. Patel, L. Zhao, P. Wong, et al., An in vitro and in vivo analysis of fibrin glue use to control bone morphogenetic protein diffusion and bone morphogenetic protein-stimulated bone growth, Spine J. 6 (4) (2006) 397–403, https://doi.org/ 10.1016/j.spinee.2005.11.006.
- [12] Q. Li, B. Tang, X. Liu, et al., Overcoming the dilemma of in vivo stable adhesion and sustained degradation by the molecular design of polyurethane adhesives for bone fracture repair, Adv. Healthcare Mater. 13 (5) (2024) 2301870, https://doi. org/10.1002/adhm.202301870.
- [13] X. Zhao, J. Ding, C. Xuan, et al., High-strength bone polyurethane adhesive with rapid curing for bone tissue injury repair, J. Mater. Chem. B 13 (17) (2025) 5150–5162, https://doi.org/10.1039/D4TB02390K.
- [14] E.A. Abou Neel, V. Salih, P.A. Revell, A.M. Young, Viscoelastic and biological performance of low-modulus, reactive calcium phosphate-filled, degradable, polymeric bone adhesives, Acta Biomater. 8 (1) (2012) 313–320, https://doi.org/ 10.1016/j.actbio.2011.08.008.
- [15] M.J. Sánchez-Fernández, J. Rutjes, et al., Bone-adhesive hydrogels based on dual crosslinked poly (2-Oxazoline)s, Macromol. Biosci. 21 (12) (2021) 2100257, https://doi.org/10.1002/mabi.202100257.
- [16] F. Baino, E. Fiume, Elastic mechanical properties of 45S5-Based bioactive glass-ceramic scaffolds, Materials 12 (19) (2019) 3244, https://doi.org/10.3390/ ma12193244.
- [17] X. Hou, L. Zhang, Z. Zhou, et al., Calcium phosphate-based biomaterials for bone repair, J. Funct. Biomater. 13 (4) (2022) 187, https://doi.org/10.3390/ ifb13040187.
- [18] M.P. Ginebra, M. Espanol, Y. Maazouz, et al., Bioceramics and bone healing, EFORT Open Rev. 3 (5) (2018) 173–183, https://doi.org/10.1302/2058-5241-317056
- [19] M. Okada, A. Nakai, E.S. Hara, et al., Biocompatible nanostructured solid adhesives for biological soft tissues, Acta Biomater. 57 (2017) 404–413, https://doi.org/ 10.1016/j.actbio.2017.05.014.
- [20] M. Okada, S.C. Xie, Y. Kobayashi, et al., Water-mediated On-Demand detachable solid-state adhesive of porous hydroxyapatite for internal organ retractions, Adv. Healthcare Mater. 13 (19) (2024) 2304616, https://doi.org/10.1002/ adhm 202304616
- [21] P.N. Christy, S.K. Basha, V.S. Kumari, et al., Biopolymeric nanocomposite scaffolds for bone tissue engineering applications—A review, J. Drug Deliv. Sci. Technol. 55 (2020) 101452, https://doi.org/10.1016/j.jddst.2019.101452.
- [22] N. Rosa, M.F.S.F. Moura, S. Olhero, et al., Bone: an outstanding composite material, Appl. Sci. 12 (7) (2022) 3381, https://doi.org/10.3390/app12073381.
- [23] X. Wang, S. Xu, S. Zhou, et al., Topological design and additive manufacturing of porous metals for bone scaffolds and orthopaedic implants: a review, Biomaterials 83 (2016) 127–141, https://doi.org/10.1016/j.biomaterials.2016.01.012.
- [24] W.N. Meigel, S. Gay, L. Weber, Dermal architecture and collagen type distribution, Arch. Dermatol. Res. 259 (1) (1977) 1–10, https://doi.org/10.1007/BF00562732.
- [25] D.H. Pashley, F.R. Tay, L. Breschi, L. Tjäderhane, et al., State of the art etch-andrinse adhesives, Dent. Mater. 27 (1) (2011) 1–16, https://doi.org/10.1016/j. dental.2010.10.016.
- [26] S. Pang, F.Y. Su, A. Green, et al., Comparison of different protocols for demineralization of cortical bone, Sci. Rep. 11 (1) (2021) 7012, https://doi.org/ 10.1038/s41598-021-86257-4.
- [27] A. Cho, S. Suzuki, J. Hatakeyama, et al., A method for rapid demineralization of teeth and bones, Open Dent. J. 4 (2010) 223, https://doi.org/10.2174/ 1874210601004010223.

- [28] H. Heidari, A. Mohammadbeigi, A. Soltanzadeh, et al., Respiratory effects of occupational exposure to low concentration of hydrochloric acid among exposed workers, Med. Gas Res. 9 (4) (2019) 208–212, https://doi.org/10.4103/2045-0012 273058
- [29] J. Sigurdsson, A. Björnsson, S.T. Gudmundsson, Formic acid burn—Local and systemic effects report of a case, Burns 9 (5) (1983) 358–361, https://doi.org/ 10.1016/0305-4179(83)90084-0.
- [30] H. Bonney, A. Goodman, Validity of the use of porcine bone in forensic cut mark studies, J. Forensic Sci. 66 (1) (2020) 278–284, https://doi.org/10.1111/1556-4029.14599.
- [31] F. Saulnier, T. Ondarçuhu, A. Aradian, et al., Adhesion between a viscoelastic material and a solid surface, Macromolecules 37 (3) (2004) 1067–1075, https://doi.org/10.1021/ma021759t.
- [32] T. Kawamoto, Use of a new adhesive film for the preparation of multi-purpose fresh-frozen sections from hard tissues, whole-animals, insects and plants, Arch. Histol. Cytol. 66 (2) (2003) 123–143, https://doi.org/10.1679/aohc.66.123.
- [33] S.V. Palagummi, F.A. Landis, M.Y.M. Chiang, Real-time synchronous measurement of curing characteristics and polymerization stress in bone cements with a cantilever-beam based instrument, Rev. Sci. Instrum. 89 (3) (2018) 035102, https://doi.org/10.1063/1.5025476.
- [34] H.I. Roach, G. Mehta, R.O.C. Oreffo, et al., Temporal analysis of rat growth plates: cessation of growth with age despite presence of a physis, J. Histochem. Cytochem. 51 (3) (2003) 373–383, https://doi.org/10.1177/002215540305100312.
- [35] J.L. Schriefer, A.G. Robling, S.J. Warden, et al., A comparison of mechanical properties derived from multiple skeletal sites in mice, J. Biomech. 38 (3) (2005) 467–475, https://doi.org/10.1016/j.jbiomech.2004.04.020.
- [36] R.D. Adams, N.A. Peppiatt, Stress analysis of adhesive-bonded lap joints, J. Strain Anal. Eng. Des. 9 (3) (1974) 185–196, https://doi.org/10.1243/ 030032473003185
- [37] E.M. Moya-Sanz, I. Ivañez, S.K. Garcia-Castillo, Effect of the geometry in the strength of single-lap adhesive joints of composite laminates under uniaxial tensile load, Int. J. Adhesion Adhes. 72 (2017) 23–29, https://doi.org/10.1016/j. ijadhadh.2016.10.009.
- [38] M. Sharabi, Structural mechanisms in soft fibrous tissues: a review, Front. Mater. 8 (2021) 793647, https://doi.org/10.3389/fmats.2021.793647.
- [39] A.T. Hexter, S. Shahbazi, T. Thangarajah, et al., Characterisation of the tensile properties of demineralised cortical bone when used as an anterior cruciate ligament allograft, J. Mech. Behav. Biomed. Mater. 110 (2020) 103981, https://doi.org/10.1016/j.jmbbm.2020.103981.
- [40] E. Gruskin, B.A. Doll, F.W. Futrell, et al., Demineralized bone matrix in bone repair: history and use, Adv. Drug Deliv. Rev. 64 (12) (2012) 1063–1077, https://doi.org/ 10.1016/j.addr.2012.06.008.
- [41] V. Sabolová, A. Brinek, V. Sládek, The effect of hydrochloric acid on microstructure of porcine (sus scrofa domesticus) cortical bone tissue, Forensic Sci. Int. 291 (2018) 260–271, https://doi.org/10.1016/j.forsciint.2018.08.030.
- [42] S. Danilchenko, A. Kalinkevich, M. Zhovner, X-ray diffraction studies of a partially demineralized oriented cortical bone with the controlled depth of analysis, Heliyon 9 (7) (2023) e17809, https://doi.org/10.1016/j.heliyon.2023.e17809.
- [43] A.B. Castro-Ceseña, E.E. Novitskaya, P.Y. Chen, Kinetic studies of bone demineralization at different HCl concentrations and temperatures, Mater. Sci. Eng. C 31 (3) (2011) 523–530, https://doi.org/10.1016/j.msec.2010.11.003.
- [44] M.R. Tatara, W. Krupski, B. Tymczyna, et al., Biochemical bone metabolism markers and morphometric, densitometric and biomechanical properties of femur and tibia in female and gonadectomised Male Polish landrace pigs, J. Pre-Clin. Clin. Res. 6 (1) (2012) 14-19
- [45] D.W. Wagner, D.P. Lindsey, G.S. Beaupre, Deriving tissue density and elastic modulus from microCT bone scans, Bone 49 (5) (2011) 931–938, https://doi.org/ 10.1016/j.bone.2011.07.021.
- [46] J.W. Mauger, Physicochemical properties of buffers used in simulated biological fluids with potential application for in vitro dissolution testing: a mini-review, dissolut, Tech 24 (3) (2017) 38–51, https://doi.org/10.14227/DT240317P38.
- [47] Y. Zhang, L. Ma, L. Cai, et al., Effects of acid concentration and the UHP pretreatment on the gelatinisation of collagen and the properties of extracted gelatins, Int. J. Food Sci. Technol. 51 (5) (2016) 1228–1235, https://doi.org/10.1111/jiifs.13089
- [48] J. Xu, F. Liu, T. Wang, H.D. Goff, F. Zhong, Fabrication of films with tailored properties by regulating the swelling of collagen fiber through pH adjustment, Food Hydrocoll. 108 (2020) 106016, https://doi.org/10.1016/j. foodhyd.2020.106016.
- [49] Y.J. Park, G.J. Choi, S.H. Kim, et al., Nanoscale characterization of acid and thermally treated collagen fibrils, Acta Biomater. 8 (9) (2012) 3381–3391, https:// doi.org/10.1016/j.actbio.2012.05.029.
- [50] W. Zhang, X. Luo, L. Niu, et al., Biomimetic intrafibrillar mineralization of type I collagen with intermediate precursors-loaded mesoporous carriers, Sci. Rep. 5 (1) (2015) 11199, https://doi.org/10.1038/srep11199.
- [51] M.R. Carrilho, F.R. Tay, A.M. Donnelly, et al., Host-derived loss of dentin matrix stiffness associated with solubilization of collagen, J. Biomed. Mater. Res. B Appl. Biomater. 90 (1) (2009) 373–380, https://doi.org/10.1002/jbm.b.31295.
- [52] C. Petibois, G. Gouspillou, K. Wehbe, et al., Analysis of type I and IV collagens by FT-IR spectroscopy and imaging for a molecular investigation of skeletal muscle connective tissue, Anal. Bioanal. Chem. 386 (2006) 1961–1966, https://doi.org/ 10.1007/s00216-006-0828-0.
- [53] H. Ping, W. Wagermaier, N. Horbelt, et al., Mineralization generates megapascal contractile stresses in collagen fibrils, Science 376 (6589) (2022) 188–192, https://doi.org/10.1126/science.abm2664.

- [54] K. Zheng, J. Zhong, J. Hu, et al., Effects of mineralization on the hierarchical organization of Collagen—a synchrotron X-ray scattering and polarized second harmonic generation study, Interface Focus 14 (3) (2024) 20230046, https://doi. org/10.1098/rsfs.2023.0046.
- [55] J. Chen, C. Burger, C.V. Krishnan, et al., In vitro mineralization of collagen in demineralized fish bone, Macromol. Chem. Phys. 206 (1) (2005) 43–51, https://doi.org/10.1002/macp.200400066.
- [56] B.D. Quan, E.D. Sone, Structural changes in collagen fibrils across a mineralized interface revealed by cryo-TEM, Bone 77 (2015) 42–49, https://doi.org/10.1016/j. bone.2015.04.020.
- [57] F.S. Utku, The consequences of dehydration-hydration on bone anisotropy and implications on the sublamellar organization of mineralized collagen fibrils, J. Biomech. 104 (2020) 109737, https://doi.org/10.1016/j. ibiomech.2020.109737.
- [58] M. Tanaka, T. Hayashi, S. Morita, The roles of water molecules at the biointerface of medical polymers, Polym. J. 45 (7) (2013) 701–710, https://doi.org/10.1038/ pi.2012.229.
- [59] A. Barth, Infrared spectroscopy of proteins, Biochim. Biophys. Acta Bioenerg. 1767(9) (2007) 1073–1101, https://doi.org/10.1016/j.bbabio.2007.06.004.
- [60] M. Vassaux, Heterogeneous structure and dynamics of water in a hydrated collagen microfibril, Biomacromolecules 25 (8) (2024) 4809–4818, https://doi.org/ 10.1021/acs.biomac.4c00183.
- [61] S. Kudo, S. Nakashima, Water retention capabilities of collagen, gelatin and peptide as studied by IR/QCM/RH system, Spectrochim. Acta Mol. Biomol. Spectrosc. 241 (2020) 118619, https://doi.org/10.1016/j.saa.2020.118619.
- [62] W. Long, L. Peng, J. Li, et al., On the role of water in regulating the mechanics of collagen fibers, Colloids Surf. A Physicochem. Eng. Asp. 702 (2024) 134957, https://doi.org/10.1016/j.colsurfa.2024.134957.

- [63] Y. Hosoya, F.R. Tay, Bonding ability of 4-META self-etching primer used with 4-META/MMA-TBB resin to enamel and dentine: primary vs permanent teeth, J. Dent. 42 (4) (2014) 425–431, https://doi.org/10.1016/ji.jdent.2014.01.007.
- [64] M.S. Razzaque, Phosphate toxicity: new insights into an old problem, Clin. Sci. 120 (3) (2011) 91–97, https://doi.org/10.1042/CS20100377.
- [65] E.M. Caravati, Metabolic abnormalities associated with phosphoric acid ingestion, Ann. Emerg. Med. 16 (8) (1987) 904–906, https://doi.org/10.1016/S0196-0644 (87)80532-2.
- [66] O. Edwards, E. Huffman, Viscosity of aqueous solutions of phosphoric acid at 25°C, Ind. Eng. Chem. Chem. Eng. Data 3 (1) (1958) 145–146, https://doi.org/10.1021/ i460003a028.
- [67] T. Dehne, R. Zehbe, J.P. Krüger, et al., A method to screen and evaluate tissue adhesives for joint repair applications, BMC Muscoskelet. Disord. 13 (1) (2012) 175, https://doi.org/10.1186/1471-2474-13-175.
- [68] Y. Chen, J. Wu, F. Li, et al., Creating a box-cavity defect model in the cortical bone of Rat Femora, J. Vis. Exp. 201 (2023) e66068, https://doi.org/10.3791/66068.
- [69] M. Li, A. Zhang, J. Li, Et, al., Osteoblast/fibroblast coculture derived bioactive ECM with unique matrisome profile facilitates bone regeneration, Bioact. Mater. 5 (4) (2020) 938–948, https://doi.org/10.1016/j.bioactmat.2020.06.017.
- [70] J.R. Dwek, The periosteum: what is it, where is it, and what mimics it in its absence? Skelet. Radiol. 39 (4) (2010) 319–323, https://doi.org/10.1007/s00256-009-0849-9.
- [71] M. Folkman, A. Becker, I. Meinster, et al., Comparison of bone-to-implant contact and bone volume around implants placed with or without site preparation: a histomorphometric study in rabbits, Sci. Rep. 10 (1) (2020) 12446, https://doi. org/10.1038/s41598-020-69455-4.
- [72] A. Noori, S.J. Ashrafi, R. Vaez-Ghaemi, et al., A review of fibrin and fibrin composites for bone tissue engineering, Int. J. Nanomed. 12 (2017) 4937–4961, https://doi.org/10.2147/IJN.S124671.